NANO LETTERS
LETTER
pubs.acs.org/NanoLett

Quantum Point Contact Microscopy

Yong-hui Zhang,*[†,‡] Peter Wahl,*[†] and Klaus Kern[†,§]

[†]Max-Planck-Institut für Festkörperforschung, Heisenbergstrasse 1, 70569 Stuttgart, Germany
[‡]Department of Physics, Tsinghua University, Beijing 100084, China
[§]Institut de Physique de la Matière Condensée, Ecole Polytechnique Fédérale de Lausanne (EPFL), CH-1015 Lausanne, Switzerland

Supporting Information

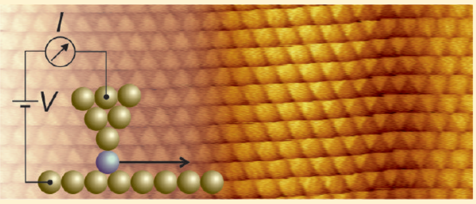

ABSTRACT: We introduce quantum point contact microscopy (QPCM) as a novel method for surface characterization, where the conductance through a quantum point contact formed by a metal atom between the tip of a scanning tunneling microscope and the surface is mapped across the surface. Application of QPCM to copper and gold (111) shows reproducibly atomic resolution, on gold (111) the alternating atomic stacking of the surface reconstruction is observed in real space. The perspectives for chemical sensitivity in QPCM images are demonstrated for an iron−platinum surface alloy where we observe local variations of the transport current due to changes in the chemical environment of the point contact.

KEYWORDS: Scanning tunneling microscopy, chemical sensitivity, atomic resolution, quantum transport

Scanning tunneling microscopy (STM) relies on probing a conductive surface in the evanescent tail of electronic states.[1,2] Due to the tip−sample distance of a few angstroms at which an STM is usually operated, STM images reflect a contour of constant density of states of the nearly unperturbed surface but often carry little information about the local chemistry. Decreasing the tip−sample distance, the sensitivity to chemical interactions can be enhanced as has been demonstrated in noncontact atomic force microscopy (AFM), where the oscillating tip comes for short periods of time within the range of chemical interactions.[3,4]

STM is usually performed in the tunneling regime with a conductance between tip and sample far below a conductance quantum ($G_0 = 2e^2/h = 77.5\,\mu S$).[5] When the STM tip approaches a metal surface in vacuum, the conductance rises exponentially with decreasing tip−sample distance in the tunneling regime and exhibits a sudden reduction in slope when the point contact regime is reached.[6,7] In this regime the conductance of the tip−sample junction is typically on the order of $\sim 1G_0$ for metal atoms on metal surfaces,[6,8,9,12] indicating that the electronic transport is governed by a small number of conduction channels through the atomic contact. The reversible and reproducible formation of single atomic contacts has been successfully demonstrated in low temperature STM for single xenon[7] as well as metal atoms.[8,9,12]

It turns out that at conductances around 1 conductance quantum and larger, well in the contact regime, the STM tip can still be scanned across the surface in a mode coined point contact microscopy (PCM). In PCM, the tip is scanned at high conductance and constant height across the surface while the current is recorded. Imaging by PCM has been demonstrated first for graphite[10] and later on epitaxial graphene on Pt(111)[11] for a wide range of conductances. However the junctions apparently did not consist of single atoms rather exhibiting a more complex geometry,[11] complicating the interpretation of the images. Quantum point contact microscopy (QPCM) is performed with a well-defined point contact consisting of a single atom between the tip and the surface. From STM images recorded before QPCM imaging, the atom forming the point contact while imaging can be selected; reversible and reproducible formation of the point contact ensures that tip and surface stay intact during QPCM imaging. The conductance while approaching the tip toward the adatom exhibits a clear transition between tunneling and contact regime at a conductance on the order of 1 conductance quantum, confirming that a single atom forms the contact. The high level of control of the single atomic contact facilitates an interpretation of QPCM images in terms of the local chemical environment of the contact atom.

Imaging by QPCM relies on a similar mechanism at the contact as "manipulated atom imaging", where an adatom is laterally manipulated by the STM tip while imaging in *constant-current* mode at conductances ranging from $0.07G_0$ to $0.26G_0$. Manipulated atom imaging has been reported for Cu(111)[16] and Ag(111)[17] surfaces and similar to QPCM reveals the binding sites of the (111) surface lattice. In contrast to manipulated atom imaging, QPCM images are acquired in *constant-height* mode and the average conductance can reach beyond $1G_0$. Because the tip−sample distance stays constant during imaging, a comparison of the conductance to theoretical calculations is greatly facilitated allowing for an interpretation in terms of the chemical environment. In manipulated atom imaging, the feedback loop keeps the current constant by adjusting the tip−sample distance which is much more complicated to account for in calculations. Recently, constant current imaging at conductances similar to

Received: June 6, 2011
Revised: July 21, 2011
Published: July 26, 2011

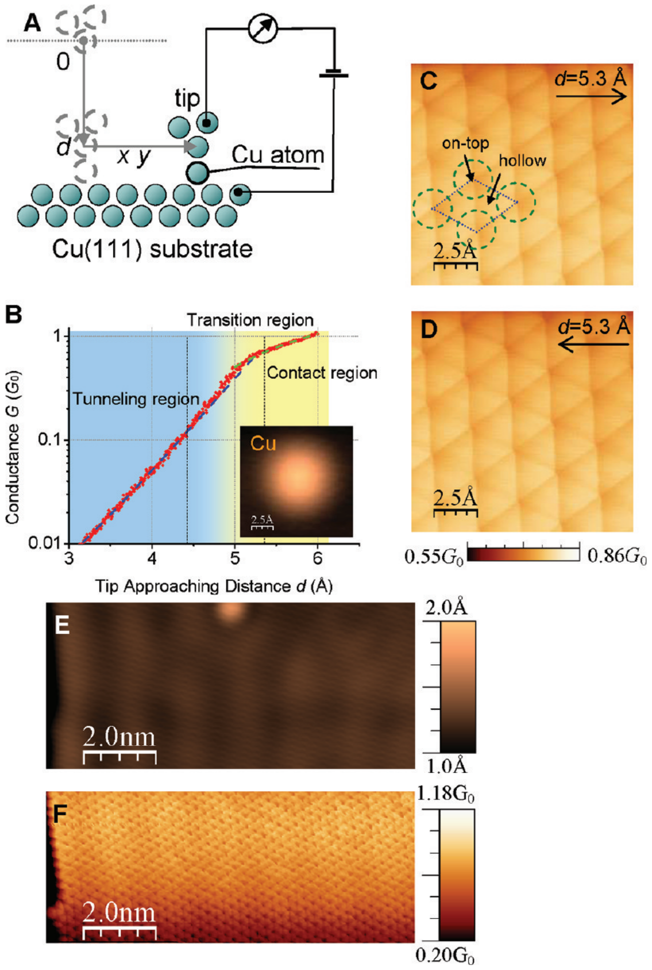

Figure 1. Illustration of QPCM on a Cu(111) surface. (A) Schematic model demonstrating the working principle of QPCM. The gray circles and arrows indicate the motion of the tip and the Cu atomic contact. (B) Conductance G as a function of tip approaching distance d acquired with the tip on top of a Cu adatom starting from a tunneling set point of $U = 105$ mV, $I = 0.11$ nA before switching off the feedback loop. The conductance data are fitted with an exponential function in the tunneling regime and with a linear function in the point contact regime. Both functions are shown with dashed lines and intersect in the transition region, where the conductance data deviate from the fitting curves. The inset shows a constant current image of a single Cu adatom on the flat Cu(111) surface (13 Å × 13 Å, $U_{\text{bias}} = 105$ mV, $I = 0.11$ nA). (C) QPCM image with the same scan size as the inset in (B), the forward scan (from left to right) is shown, acquired after the feedback loop has been switched off at $U_{\text{bias}} = 105$ mV, $I = 0.11$ nA, and the tip approached by $d = 5.3$ Å on top of the Cu adatom. The circles indicate the positions of the copper atoms in the surface layer; the diamond depicts a surface unit cell. The conductance image was acquired in constant height mode ($U_{\text{bias}} = 105$ mV, scanning speed 154 Å/s). A slight increase in conductance from top to bottom is observed due to piezo creep during scanning. (D) Backward scan (from right to left) acquired simultaneously with the image shown in (C). (E) Constant current image of a step edge on Cu(111) ($U_{\text{bias}} = 13$ mV, $I = 0.11$ nA). Standing wave patterns originating from the surface state are clearly visible in the image. (F) QPCM image of the same area as shown in (E) ($U_{\text{bias}} = 13$ mV, $d = 4.0$ Å with respect to a tunneling set point of $U_{\text{bias}} = 13$ mV, $I = 0.11$ nA). The conductance decrease from top to bottom of the image is due to the plane in which the tip scans being slightly tilted with respect to the surface.

what we employ for QPCM has been demonstrated on a Pb thin film on Ag(111) without an adatom to form the contact.[28] In this case, the tip atom reversibly forms the contact, which appears to be a special property of the Pb film.

After introducing the method, we will first present QPCM imaging of the Cu(111) surface as a function of conductance to establish the basic imaging mechanism of QPCM on noble metal surfaces. As a demonstration of the potential of QPCM, imaging of the herringbone reconstruction of Au(111) revealing structural information beyond the topmost surface layer is shown. Finally, QPCM imaging of an FePt surface alloy demonstrates potential chemical sensitivity of the method. Experiments have been performed in a home-built ultrahigh vacuum (UHV)-STM operating at a sample temperature of ~6.7 K. The basic measurement procedure is sketched in Figure 1A (for details see S1, Supporting Information): QPCM images are acquired by first positioning the tip on top of an adatom, here a copper atom, which will form the atomic contact (Figure 1B inset). The tip is approached with the feedback loop switched off by a predefined distance d toward the surface to establish contact. The conductance G as a function of tip approaching distance d shown in Figure 1B clearly shows the vacuum tunneling and point contact regime separated by a transition region. The contact is then scanned across the surface in constant height mode while recording the current. Upon completion of imaging the junction atom is left on the surface where the tip withdraws.

QPCM images of the Cu(111) surface are shown in panels C and D of Figure 1; they reveal a hexagonal lattice with a lattice constant close to that of copper. From lattice symmetry arguments, the triangular areas in the QPCM images are attributed to the hollow sites of the Cu(111) surface and the dark spots surrounded by six triangular areas are attributed to on-top sites. The periodic structure found in QPCM images can be explained by the copper atom which forms the point contact always staying in the hollow site closest to the apex of the tip, as is similarly reported for the manipulated atom imaging.[16] This is a result of a potential well induced by the presence of the tip due to the interaction between the tip and the adatom at small tip–surface distances which traps the adatom at the hollow sites closest to the tip.[15,16] Consequently, the triangular shape is due to the atom hopping to the next hollow site whenever the tip crosses the boundary between adjacent hollow sites. The coincidence of QPCM images recorded with opposite scan directions as shown in panels C and D of Figure 1 as well as their stable conductance profiles are strong evidence that, at ~$0.75G_0$, on the time scale of our measurement the copper atomic contact always stays at the energetically favored binding site imposed by the tip position, and transition rates between adjacent sites are beyond the time resolution (10^{-4}s) of our measurement.

In contrast, conductance fluctuations from 10 to 10^4 Hz were observed in manipulated atom images acquired in constant current mode at conductances ranging from $0.07G_0$ to $0.26G_0$[16] due to hopping of the adatom between adjacent hollow sites. The transition rate was found to increase at smaller tip–sample distances due to a lowering of the energy barrier for lateral translation. Considering that QPCM images in Figure 1 are acquired at significantly smaller tip–sample distance than manipulated atom images, the energy barrier of lateral translation of the copper atomic contact between adjacent hollow sites on the Cu(111) surface can be expected to be rather small, which leads to a high transition rate, consistent with the lack of conductance fluctuations in our data.

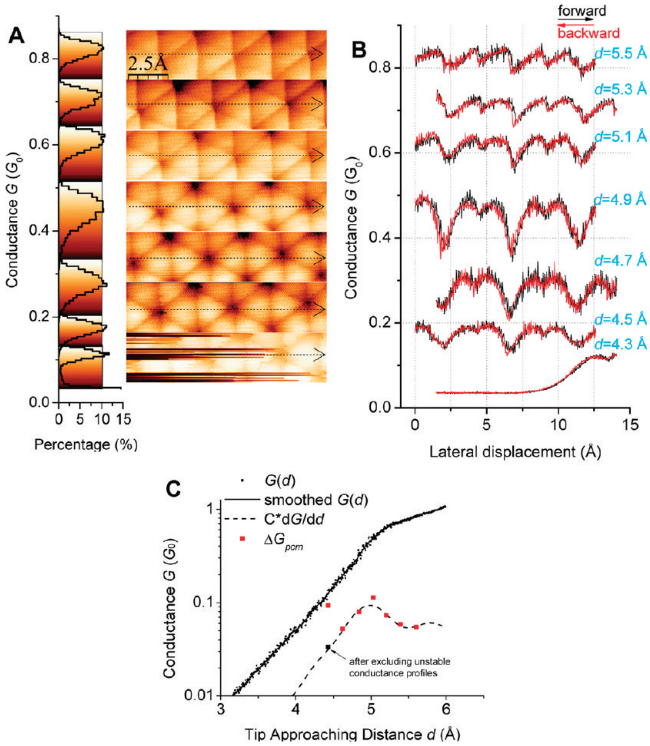

Figure 2. QPCM of copper (111) at different conductances. (A) QPCM images (scanned from left to right) acquired at average conductances ranging from $0.85G_0$ at the top to $\sim 0.1G_0$ at the bottom (scan parameters are identical to Figure 1C except for the tip approaching distance d and image size 13×3.2 Å^2). Histograms of each image are shown on the left together with the color bars. (B) Pairs of forward (black) and backward (red) scan lines across a few on-top sites for each QPCM image in (A) acquired at different tip approaching distances d. Positions of the scan lines are indicated by a dashed arrow on each QPCM image. Images shown here and in Figure 1 have all been acquired with the same tip. (C) Comparison between the derivative of the tip approach curve in Figure 1B (dG/dd, black dashed line) and the width of the conductance histogram of QPCM images in (A) plotted as a function of tip approaching distance (ΔG, red squares; at $G \sim 0.1G_0$ the width ΔG after excluding unstable conductance profiles is shown as a black square), where the tip approaching distances of QPCM images are derived from the $G(d)$ curve at corresponding conductance to take into account piezo creep that tends to increase the conductance.

As is demonstrated in panels E and F of Figures 1, also defects such as step edges can be characterized and the atomic lattice close to them resolved. Figure 1E shows a tunneling image of a step edge showing little contrast on the terrace. The QPCM image in Figure 1F shows the lattice structure up to the step edge, where the contact is lost when the tip moves from the upper toward the lower terrace and is regained when the tip returns.

To better understand QPCM of metal surfaces, we have studied QPCM images as a function of conductance from $\sim 0.1G_0$ to $\sim 1G_0$, as shown in Figure 2A and Figure 2B. For small conductances $G \sim 0.1G_0$, QPCM becomes unstable as the copper adatom does not reliably follow the tip indicating that the transition rate of the atom between adjacent binding sites becomes too low. In the conductance range from $0.15G_0$ to $0.85G_0$, QPCM images expose a similar structure composed of triangularly shaped areas as seen in panels C and D of Figure 1. For the lowest conductance $G \sim 0.15G_0$ for which stable imaging is shown in Figure 2, slightly different appearances of sites corresponding to a local face-centered cubic (fcc) and hexagonal close packed (hcp) stacking are found. At high conductances above $0.5G_0$, the shape of the triangular areas deviates from the 3-fold rotational symmetry of the Cu(111) surface lattice. This distortion of the patterns is tip-dependent (compare, e.g., Figure S1C, No. 6, Supporting Information) and likely due to asymmetric relaxations occurring in the apex of the tip while scanning.[18,19] The periodicity of QPCM images in Figures 1 and 2 requires the deformation of the tip apex to be reversible. In Figure 2C, the contrast in the conductance ($\Delta G_{\text{pcm}} = G_{\text{max}} - G_{\text{min}}$) of the QPCM images in Figure 2A is plotted together with the derivative of the $G(d)$ curve in Figure 1B, both are found to be roughly proportional to each other. Thus the contrast in QPCM images is governed by the slope of the $G(d)$ trace at the conductance at which the image is taken. On the basis of this observation, we have developed a simple geometrical model which describes the appearance of QPCM images (see S2, Supporting Information) as a function of conductance, which fits well particularly for conductances below $0.5G_0$ (see Figure S3B, Supporting Information) where asymmetric relaxations are negligible.

While the periodicity of QPCM images is found to coincide with that of the surface lattice, the conductance pattern depends strongly on the STM tip. Imaging with some tips yields patterns with 3-fold rotational symmetry in the tunneling regime (Figure 1, Figure 2A, and Figure S1A, Supporting Information), while for other tips even when imaging in the tunneling regime the conductance patterns deviate from the 3-fold rotational symmetry of the surface lattice (Figure S1B and Figure S1C, except No.6, Supporting Information), likely due to the tips being either asymmetric or soft. Distortion in the QPCM images can be minimized by training the tip (see S1, Figure S1, Supporting Information) to facilitate an interpretation of the data in terms of surface properties.

We succeeded in performing QPCM on Cu(111), Ag(111), Au(111), and Pt(111) surfaces despite significant differences between their diffusion barriers for adatoms. The diffusion barriers for adatoms on copper and silver (111) surfaces are rather low around 0.06 eV, whereas for a platinum atom on Pt(111) it is about 4 times larger (Cu/Cu(111), 0.057 eV; Ag/Ag(111), 0.068 eV; Pt/Pt(111), 0.26 eV).[20,21] This underlines that the diffusion barrier for adatoms is significantly reduced by the presence of the tip. A peculiarity of the Au(111) surface is the herringbone reconstruction of the clean surface,[23,24] which is formed by a uniaxial contraction of the surface layer. The reconstruction leads to regions which have been attributed to a local fcc and hcp stacking of the topmost layer with respect to the second layer, separated by a transition region where the surface atoms are close to bridge sites of the second layer.[22−24] This model for the reconstruction of the Au(111) surface was established based on transmission electron microscopy,[22] helium atom scattering,[23] and STM;[24] however, the different local stacking derived from the Au(111) reconstruction model has to our knowledge not been observed directly.

As we will show in the following, the different stackings in the two regions of the Au(111) surface result in a distinct conductance contrast in QPCM images. Figure 3A shows an STM constant-current image of the reconstructed Au(111) surface; in the image also a cobalt adatom is seen (for preparation see S3 in the Supporting Information). Pairs of ridges which form the boundaries between fcc and hcp stacked regions of the herringbone reconstruction, are clearly visible. A QPCM image acquired

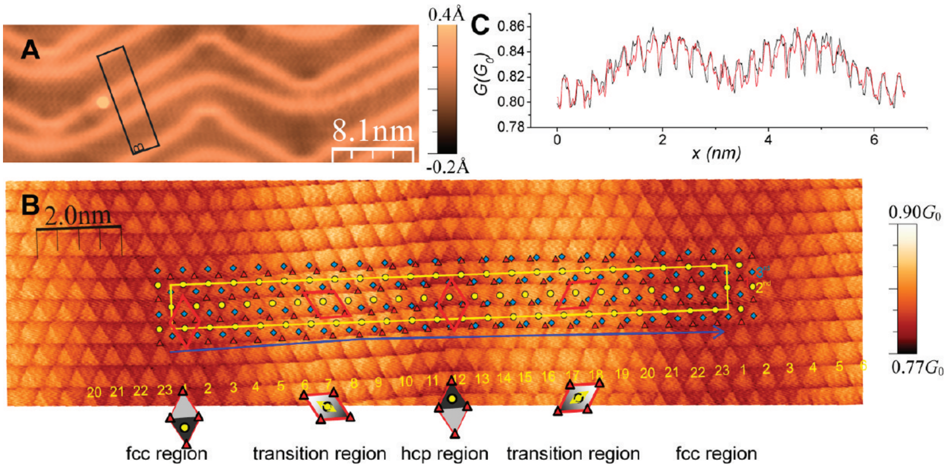

Figure 3. QPCM of the gold (111) surface reconstruction. (A) STM image of the Au(111) surface reconstruction ($U_{\text{bias}} = 100$ mV, $I = 0.10$ nA). The bright spherical blob is the Co adatom which has been used for QPCM in (B), the black rectangle indicates roughly the position and dimension of the imaging area of (B), and the letter B shows the orientation of the imaging area. (B) QPCM image (scanned from left to right, from bottom to top) of the area indicated by the rectangle in (A) ($U = 10$ mV, $G_{\text{mean}} = 0.83G_0$, scan speed 154 Å/s, size 101.1 × 25.3 Å^2). Red triangles indicate the positions of the first (top) layer Au atoms derived from the image, yellow circles and blue diamonds indicate the second and third layer Au atoms, respectively, drawn at undisturbed fcc(111) lattice sites. Their positions relative to the first layer Au atoms are determined from the stacking fault model of the Au(111) surface reconstruction in ref 23. A unit cell of the $23 \times \sqrt{3}$ surface reconstruction is indicated by a yellow rectangle. (C) Conductance line profiles along the blue arrow in (B): red line for the forward scan, black line for the backward scan (shown in Figure S4, Supporting Information). The conductance profiles of opposite scan directions differ slightly.

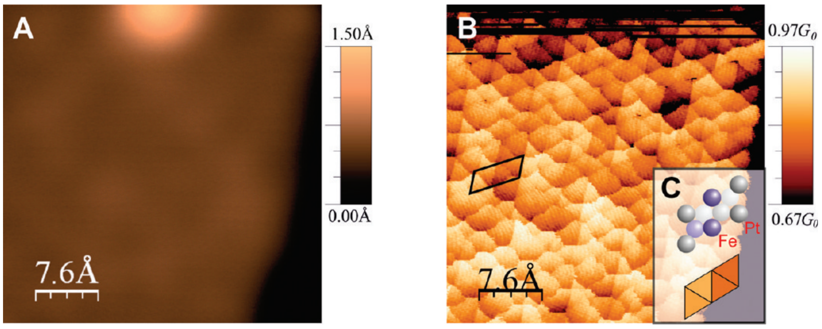

Figure 4. QPCM image of an iron−platinum surface alloy. (A) Tunneling constant current image of a step edge on the Pt(111) surface prepared with the FePt surface alloy before performing QPCM with the adatom (which has been put down from the tip) at the top-center of the image ($U_{\text{bias}} = 106$ mV, $I = 0.11$ nA). Spatial inhomogeneity observed on the terrace originates from electronic states due to the alloy. (B) QPCM image of the same area as in (A), lateral displacement of less than 1 Å with respect to (A) may exist, $U = 106$ mV, tip approaching distance $d = 4.8$ Å. A slight increase in conductance from top to bottom is found due to piezo creep during scanning. In contrast to the tunneling image in (A), the QPCM image resolves conductance differences at the atomic scale on the alloyed terrace as well as the atomic structure of the step edge. (C) Structural model of the 2 × 1 structural unit as indicated in (B) and calculated conductance pattern associated with it. The structural model derives from the 2 × 1 periodicity and consistency with LEIS and LEED data[26] as well as the coverage of iron. Atoms shown brighter are in lower layers (first three layers shown). The conductance pattern is obtained from a model calculation. Darker areas represent lower conductance (see Supporting Information for details).

in the area indicated in Figure 3A by the black rectangle is presented in Figure 3B. Besides the ridges, the QPCM image reveals a lattice of triangularly shaped hollow sites. In contrast to QPCM images shown in Figure 2, adjacent hollow sites exhibit slightly different conductances. A natural explanation of this difference is the inequivalence of fcc and hcp adsorption sites on the surface. Below fcc hollow sites there is no atom in the second layer, whereas below hcp sites there is one. As can be seen in Figure 3B, the contrast reverses when comparing the fcc and the hcp stacked regions: in the fcc stacked region, high conductance triangles point upward, while in the hcp stacked regions they point downward. In the transition regime, the contrast across the bridge site is suppressed. The contrast in conductance between adjacent hollow sites remains the same at equivalent positions of the herringbone reconstruction.

To allow for a detailed comparison with the model of the Au(111) $23 \times \sqrt{3}$ surface reconstruction,[23] in the QPCM image in Figure 3B, the positions of the gold surface atoms (first layer, denoted with red triangles) are indicated. The positions of the atoms in the second (yellow circles) and third (blue diamonds) layers are also shown, assuming that they occupy unperturbed positions in an fcc lattice. By comparison with the model, we assign higher conductance to the cobalt atomic contact being in an fcc site and lower conductance to the hcp site as sketched below Figure 3B. The QPCM image is fully consistent with the atomic model of the Au(111) $23 \times \sqrt{3}$ surface reconstruction.

QPCM images of the Au(111) surface with a gold atom serving as atomic point contact show far more distortion than with a cobalt contact, and no reproducible data have been obtained to compare with the Au(111) surface reconstruction model. Note that for QPCM images of Cu(111) taken with a copper atomic contact (Figure 2) no contrast between fcc and hcp sites is found at similar conductances. This is in contrast to manipulated atom imaging with a Co adatom on a Cu(111) surface,[16] where at much lower conductances a difference in the lateral dimension of fcc and hcp sites is observed, but no difference in conductance between the fcc and hcp sites has been reported therein.

In order to assess the influence of the local chemical environment of the point contact on the conductance, we have performed QPCM imaging on an FePt surface alloy. The FePt surface alloy is formed by deposition of Fe on a Pt(111) surface and subsequent annealing (for details see S4, Supporting Information). A tunneling image of a terrace near a step edge is shown in Figure 4A. Only some local inhomogeneities in the apparent height due to the surface alloy are apparent, whereas neither the atomic structure of the alloy nor that of the step edge is resolved. Atomic resolution of surface alloys or of structural defects by normal STM is often difficult to achieve and only possible in the presence of adsorbates in the tunneling junction.[25] Figure 4B shows a QPCM image of the same surface area. It shows the same basic lattice structure composed of triangles as found on Cu(111). However in contrast to Cu(111), the atomic scale inhomogeneity due to the surface alloy becomes apparent as the triangles centered at the hollow sites expose varying size, shape, and conductance. QPCM on clean Pt(111) shows homogeneous conductance patterns similar to Cu(111) (Figure 1C–F). The atomic scale inhomogeneity of the QPCM image of the FePt surface alloy carries information about the local chemical environment of the atomic contact. Locally, conductance patterns reminiscent of a 1 × 2 structure are found (indicated in Figure 4B by a black frame), consistent with (2 × 2) diffraction spots observed in LEED measurements of an FePt surface alloy.[26]

To relate the conductance patterns with the surface atomic structure, we have performed DFT calculations of a number of alloy configurations and tentatively calculated the conductance based on a nonequilibrium Green's function approach (for details see S5 in the Supporting Information). A comparison with previous experiments on FePt surface alloys[26] and conductance patterns extracted from the calculations allow us to single out two atomic configurations for the 1 × 2 structural unit which have the same composition (one is shown in Figure 4C, compare also S5 in the Supporting Information). We expect that a full ab initio treatment of the contact including tip, contact atom, and surface will allow identification of the surface atomic structure from the conductance pattern.

Quantum point contact microscopy provides a novel imaging mode to determine the atomic structure of conducting surfaces. It complements tunneling measurements which probe evanescent electronic states of the sample by an up-close picture, which is strongly influenced by the local atomic and chemical configuration of the topmost atomic layers as exemplarily demonstrated for the reconstruction of the gold (111) surface and an iron–platinum surface alloy. Besides performing QPCM with single atoms at the contact between tip and surface, by using molecules it might be possible to adjust the contrast of QPCM images for specific characteristics of the surface such as local reactivity or selectivity of adsorption and binding sites.

Apart from the prospect to study structural and chemical properties of a surface, QPCM can also be used as a tool to study quantum transport. Conduction through single atoms and molecules has been studied extensively both by STM[7−9,12] and mechanically controllable break junctions[13,14,27] with the vision of establishing an understanding of molecular transport for the realization of single molecule devices and electronics. QPCM adds to STM the ability to easily and quickly assess the influence of defects, surface impurities, and electronic inhomogeneities on quantum transport by scanning the contact across the electrode surface.

■ ASSOCIATED CONTENT

Ⓢ **Supporting Information.** (S1) Methods, (S2) geometrical model, (S3) QPCM on reconstructed Au(111) surface, (S4) preparation of FePt surface alloy, (S5) calculation of conductance, (S6) interpretation to the contact image of Pb wetting layer. This material is available free of charge via the Internet at http://pubs.acs.org.

■ AUTHOR INFORMATION

Corresponding Author

*E-mail: P.W., wahl@fkf.mpg.de; Y.Z., zhangyonghui02@tsinghua.org.cn.

■ ACKNOWLEDGMENT

We acknowledge discussions with W. Belzig on the NEGF calculations and U. Schlickum on QPCM experiments on Au(111). Y.Z. acknowledges support by the Chinese Scholarship Council.

■ REFERENCES

(1) Binnig, G.; Rohrer, H.; Gerber, Ch.; Weibel, E. Tunneling through a controllable vacuum gap. *Appl. Phys. Lett.* **1982**, *40*, 178–180.

(2) Binnig, G.; Rohrer, H.; Gerber, Ch.; Weibel, E. Surface Studies by Scanning Tunneling Microscopy. *Phys. Rev. Lett.* **1982**, *49*, 57–61.

(3) Giessibl, F. J.; Hembacher, S.; Bielefeldt, H.; Mannhart, J. Subatomic Features on the Silicon (111)-(7 × 7) Surface Observed by Atomic Force Microscopy. *Science* **2000**, *289*, 422–425.

(4) Sugimoto, Y.; Pou, P.; Abe, M.; Jelinek, P.; Perez, R.; Morita, S.; Custance, O. Chemical identification of individual surface atoms by atomic force microscopy. *Nature* **2007**, *446*, 64–67.

(5) Binnig, G.; Rohrer, H. Scanning Tunneling Microscopy. *Surf. Sci.* **1985**, *152/153*, 17–26.

(6) Gimzewski, J. K.; Möller, R. Transition from the tunneling regime to point contact studied using scanning tunneling microscopy. *Phys. Rev. B* **1987**, *36*, 1284–1287.

(7) Yazdani, A.; Eigler, D. M.; Lang, N. D. Off-Resonance Conduction Through Atomic Wires. *Science* **1996**, *272*, 1921–1924.

(8) Limot, L.; Kröger, J.; Berndt, R.; Garcia-Lekue, A.; Hofer, W. A. Atom Transfer and Single-Adatom Contacts. *Phys. Rev. Lett.* **2005**, *94*, 126102.

(9) Néel, N.; Kröger, J.; Berndt, R. Quantized Conductance of a Single Magnetic Atom. *Phys. Rev. Lett.* **2009**, *102*, 086805.

(10) Smith, D. P. E.; Binnig, G.; Quate, C. F. Atomic point-contact imaging. *Appl. Phys. Lett.* **1986**, *49*, 1166–1168.

(11) Enachescu, M.; Schleef, D.; Ogletree, D. F.; Salmeron, M. Integration of point-contact microscopy and atomic-force microscopy: Application to characterization of graphite/Pt(111). *Phys. Rev. B* **1999**, *60*, 16913–16919.

(12) Vitali, L.; Ohmann, R.; Stepanow, S.; Gambardella, P.; Tao, K.; Huang, R.; Stepanyuk, V. S.; Bruno, P.; Kern, K. Kondo Effect in Single Atom Contacts: The Importance of the Atomic Geometry. *Phys. Rev. Lett.* **2008**, *101*, 216802.

(13) Krans, J. M.; Muller, C. J.; Yanson, I. K.; Govaert, Th.C.M.; Hesper, R.; van Ruitenbeek, J. M. One-atom point contacts. *Phys. Rev. B* **1993**, *48*, 14721–14724.

(14) Scheer, E.; Agraït, N.; Cuevas, J. C.; Levy Yeyati, A.; Ludolph, B.; Martín-Rodero, A.; Rubio Bollinger, G.; van Ruitenbeek, J. M.; Urbina, C. The signature of chemical valence in the conduction through a single-atom contact. *Nature* **1998**, *394*, 154–157.

(15) Ternes, M.; Lutz, C. P.; Hirjibehedin, C. F.; Giessibl, F. J.; Heinrich, A. J. The Force Needed to Move an Atom on a Surface. *Science* **2008**, *319*, 1066–1069.

(16) Stroscio, J. A.; Celotta, R. J. Controlling the Dynamics of a Single Atom in Laterial Atom Manipulation. *Science* **2004**, *306*, 242–247.

(17) Sperl, A.; Kröger, J.; Berndt, R. Direct observation of conductance fluctuations of a single-atom tunneling contact. *Phys. Rev. B* **2010**, *81*, 035406.

(18) Agraït, N.; Rubio, G.; Vieira, S. Plastic Deformation of Nanometer-Scale Gold Connective Necks. *Phys. Rev. Lett.* **1995**, *74*, 3995–3998.

(19) Rubio, G.; Agraït, N.; Vieira, S. Atomic-Sized Metallic Contacts: Mechanical Properties and Electronic Transport. *Phys. Rev. Lett.* **1996**, *76*, 2302–2305.

(20) Schlösser, D. C.; Morgenstern, K.; Verheij, L. K.; Rosenfeld, G.; Besenbacher, F.; Comsa, G. Kinetics of island diffusion on Cu(111) and Ag(111) studied with variable-temperature STM. *Surf. Sci.* **2000**, *465*, 19–39.

(21) Brune, H. Microscopic view of epitaxial metal growth: nucleation and aggregation. *Surf. Sci. Rep.* **1998**, *31*, 121–229.

(22) Takayanagi, K.; Yagi, K. Monatom-High Level Electron Microscopy of Metal Surfaces. *Trans. Jpn. Inst. Met.* **1983**, *24*, 337–348.

(23) Harten, U.; Lahee, A. M.; Toennies, J. P.; Wöll, Ch. Observation of a Soliton Reconstruction of Au(111) by High-Resolution Helium-Atom Diffraction. *Phys. Rev. Lett.* **1985**, *54*, 2619–2622.

(24) Barth, J. V.; Brune, H.; Ertl, G.; Behm, R. J. Scanning tunneling microscopy observations on the reconstructed Au(111) surface: Atomic structure, long-range superstructure, rotational domains, and surface defects. *Phys. Rev. B* **1990**, *42*, 9307–9318.

(25) Schmid, M.; Stadler, H.; Varga, P. Direct Observation of Surface Chemical Order by Scanning Tunneling Microscopy. *Phys. Rev. Lett.* **1993**, *70*, 1441–1444.

(26) Jerdev, D. I.; Koel, B. E. Fe deposition on Pt(111): a route to Fe-containing Pt-Fe alloy surfaces. *Surf. Sci. Lett.* **2002**, *513*, L391–L396.

(27) Agraït, N.; Yeyati, A. L.; van Ruitenbeek, J. M. Quantum properties of atomic-sized conductors. *Phys. Rep* **2001**, *377*, 81–279.

(28) Becker, M.; Berndt, R. Conductance of atom-sized Pb contacts. *New J. Phys.* **2010**, *12*, 113010.